

## Supporting Information

# Twisted cholesterol crystals by Mueller matrix microscopy

Yue Tian, ‡<sup>a</sup> Mengyuan Hao, ‡<sup>a</sup> Yong Tang,<sup>a</sup> Chen Li,<sup>a</sup> Demei Kong,<sup>a</sup> Junru Zhu,<sup>a</sup>

Weikang Wang,<sup>a,\*</sup> Xiaoyan Cui,<sup>a,\*</sup> and Ting Wang<sup>b,c,\*</sup>

<sup>a</sup> School of Chemistry and Molecular Engineering, East China Normal University, 500 Dongchuan Road, Shanghai, China 200241

<sup>b</sup> Shanghai Skin Disease Hospital, School of Medicine, Tongji University, 1278 Baode Road, Shanghai, China, 200443

<sup>c</sup> Shanghai Engineering Research Center of Topical Chinese Medicine, 1278 Baode Road, Shanghai, China, 200443

\* Email: wangting1983927@gmail.com; xycui@chem.ecnu.edu.cn;  
wkwang@chem.ecnu.edu.cn

# Table of Content

## Contents

1. Materials, Methods and Characterization
2. Muller Matrix Experiment and Simulation
3. Calculation Details
4. Supplementary Figures

Fig. S1. Polarized optical micrographs of cholesterol spherulites

Fig. S2. SEM images of cholesterol polymorph I

Fig. S3. SEM images of cholesterol polymorph II

Fig. S4. SEM images of cholesterol monohydrate spherulite

Fig. S5. Experimental and simulated optical results of banded cholesterol polymorph I

Fig. S6. Experimental and simulated optical results of banded cholesterol polymorph II

Fig. S7. Experimental optical results of monohydrate cholesterol spherulites

Fig. S8. Stained cholesterol banded spherulites and their corresponding fluorescent images

Fig. S9. Experimental and simulated optical results of stained banded cholesterol polymorph

5. Reference

## **1. Materials, Methods and Characterization**

### **Materials**

All reagents were analytical grade purchased from standard suppliers and used without further purification. Cholesterol used in this work was purchased from Adamas-beta. Polyvinylpyrrolidone (PVP) was purchased from Sigma. Nile red was purchased from Adamas-life.

### **Methods**

**Fabrication of anhydrous cholesterol banded spherulites.** PVP (15 wt.%) powder and cholesterol (85 wt.%) were well mixed. 2.0 mg of the mixture was placed on a glass slide and covered with a cover glass. The glass slide was placed on a hot stage, and the temperature was raised to 180 °C. The powder was dissolved into liquid at 20 °C/min. Banded spherulites grew at 120 °C for 20 min.

**Fabrication of stained anhydrous cholesterol banded spherulites.** 1.0 wt.% lipophilic fluorophores were premixed with cholesterol powder doped with 15 wt.% PVP. Then, the spherulites are grown according to the aforementioned procedures.

**Fabrication of monohydrate cholesterol spherulites.** The preparation method for cholesterol globules in one water is as follows: 200 mg cholesterol powder is dissolved in 20 mL ethanol. 200 mL distilled water is added drop-wise to the solution for a hydrated ethanol solution of cholesterol. 2.0 g of poly(vinyl)alcohol (PVA) was dissolved in 100 mL water at 95 °C and cooled to room temperature. PVA gel was heated to 70 °C before the cholesterol solution was dropped into a gel. After about 1 min, cholesterol monohydrate spherulites appeared.

### **Characterizations**

Cholesterol-banded spherulites crystalized on a hot stage (Linkam, LTS420) from the melts. Optical micrographs were taken with a polarized optical microscope (POM, Leica DM750) equipped with a digital camera (Nikon, D800). The spherulites were analyzed with the X-ray powder diffraction apparatus (Rigaku, MiniFlex 600). The  $2\theta$  were recorded from 5 to 25° with a step size of 0.02°. Raman spectra were collected

by a Raman spectrometer (Renishaw, Invia) equipped with a 633 nm laser in mapping mode (100% energy excitation and exposure time are 10 s). Scanning electron microscopy (SEM, Hitachi, S-4800) was used to characterize the microstructure of the spherulites. The samples were sputter-coated with gold (10.0 nm) before evaluation and the scanning voltage is 3.0 kV.

## 2. Muller Matrix Experiment and Simulation

**Experiment.** Mueller matrix microscopy (MMM) images were obtained using a home-built Mueller matrix polarimeter.<sup>1</sup> Before the measurement, we calibrate the system by comparing the measurement results of known standard samples (air) with their theoretical values. The numerical aperture of the objective was 0.28, and the wavelength of the incident light was 530 nm for the unstained cholesterol crystals and 550 nm for the stained cholesterol spherulites.

**Simulation.** In banded spherulites, the |LB| for each crystalline fiber, along with the misalignment angle between adjacent fibers, is essential for simulating the CB. For polymorph I, it has been assumed that a bundle of crystal fibers consists of 20 lamellae based on SEM data. Consequently, the parameters are  $P=20$ , total misalignment  $\Psi=20^\circ$ , and the refractive index vector of lamella  $[n_x, n_y, n_z] = [1.549, 1.536, 1.519]$ . For polymorph II, the parameters are  $P=30$ ,  $[n_x, n_y, n_z] = [1.581, 1.548, 1.564]$ , and total misalignment  $\Psi=25^\circ$ .

The |LD| and CD can indicate the absorption of the spherulite. The stimulation of |LD| and CD also requires specific parameters related to the dye ( $B$ ,  $\Phi_{dye}$ , and  $\Theta_{dye}$ ).  $B$  is a wavelength-dependent complex-valued oscillator amplitude. Each oscillator contributes to the total permittivity through a dyadic tensor defined by the outer product  $\otimes$ , which is scaled by  $B$ .  $B(u \otimes u)$  generates the differential Mueller matrix parameters  $L_1$  (LD),  $L_2$  (LD'), and  $L_3$  (CD). The real part of  $B$  represents the contribution to dispersion and should be expressed as a negative value for the sign convention requires, while the imaginary part is associated with the absorption of light by the dye. A comprehensive explanation of the theoretical simulation principles is described in

the reference [10.1021/jacs.6b06278].<sup>2</sup> In the case of unstained CC, no light can be absorbed, resulting in  $B = 0$ .

### 3. Calculation Details

The geometry of coumarin was optimized by density functional theory (DFT) calculations with Gaussian 16 program at B3LYP/6-311G(d) level. The optimized structures were further employed in the adsorption energy on the (001), (010), (100), ( $1\bar{1}0$ ) and ( $01\bar{1}$ ) surfaces of anhydrous cholesterol crystal (polymorphs II) with dreiding force field. After expanding into the  $3 \times 3$  supercell of anhydrous cholesterol crystal, the five main planes were cleaved and then installed a 30 Å vacuum box. The energetically preferred adsorbed configuration was evaluated by simulated annealing calculations employing the stochastic Monte Carlo method with geometric optimization. The cholesterol molecules were constrained while only the adsorbate was allowed to relax, and the whole system was optimized geometrically. Then adsorption energy of the whole system was calculated after releasing the cholesterol molecules ( $E_{\text{surface+adsorbate}}$ ). The energy of the crystal surface ( $E_{\text{surface}}$ ) and the adsorbate ( $E_{\text{adsorbate}}$ ) was evaluated by manually removing the adsorbate molecule or crystallin structure. The adsorption energy of dye on each crystal surface is calculated according to the following formula:<sup>3</sup>

$$E_{\text{adsorption}} = E_{\text{surface+adsorbate}} - (E_{\text{surface}} + E_{\text{adsorbate}})$$

#### 4. Supplementary Figures

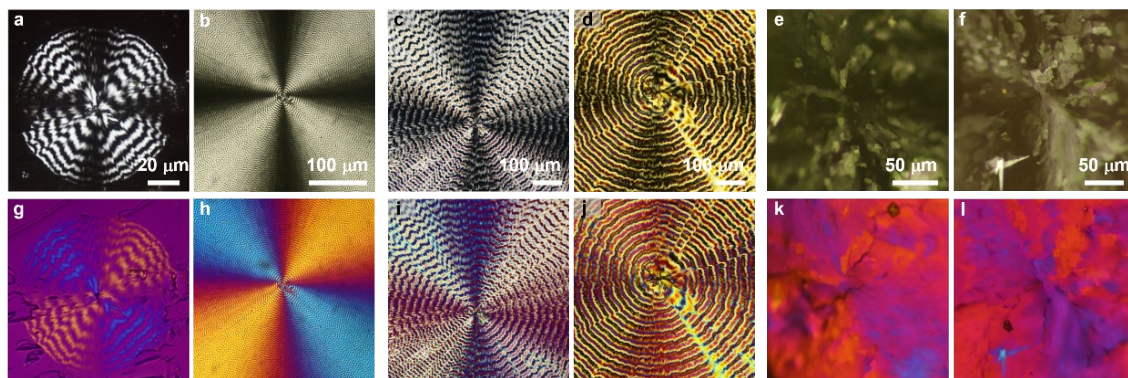


Fig. S1 Polarized optical micrographs of cholesterol spherulites. (a-b) POM images of anhydrous cholesterol banded spherulites polymorph I. (c-d) POM images of anhydrous cholesterol banded spherulites polymorph II. (e-f) POM images of monohydrate cholesterol spherulites. (g-l) POM images with crossed-polarizers and retarders.

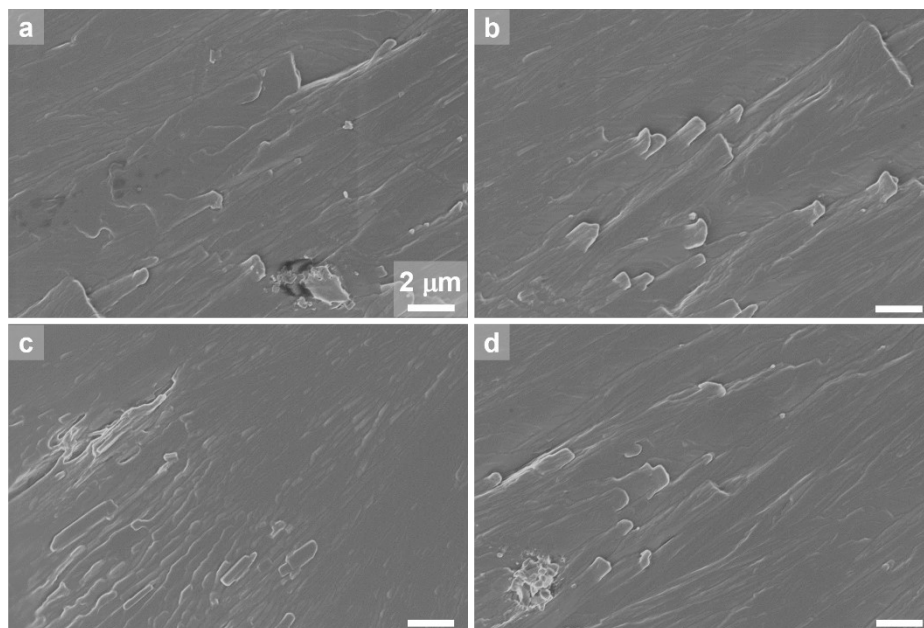


Fig. S2 SEM images of cholesterol polymorph I.

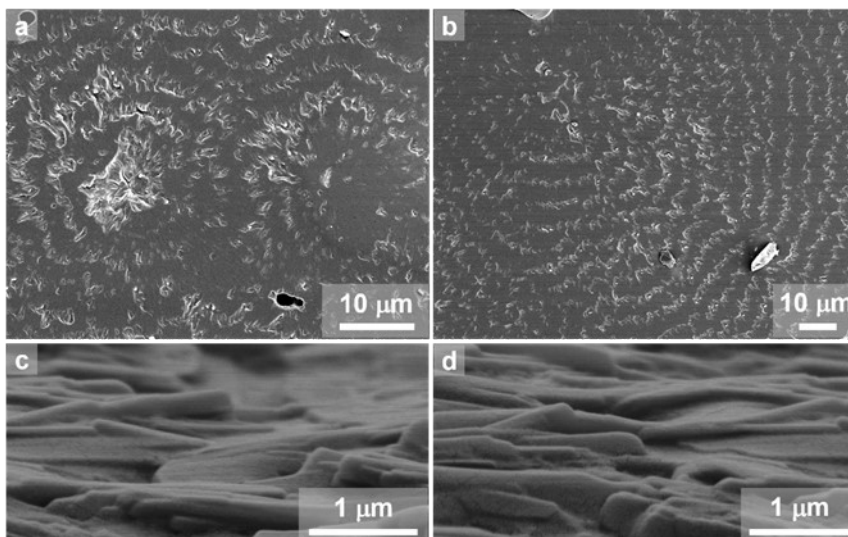


Fig. S3 SEM images of cholesterol polymorph II. (a-b) Microscopic morphology of polymorph II. (c-d) Helical fibers in cross-sectional SEMs of polymorph II.



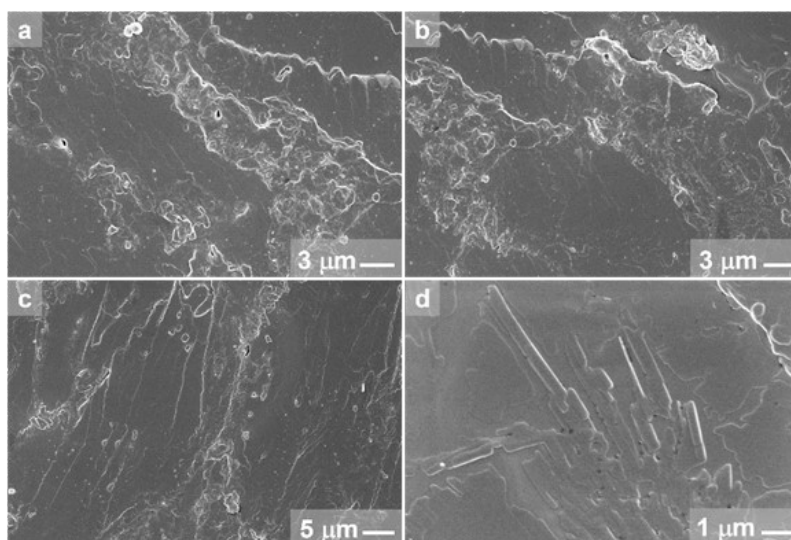


Fig. S4 SEM images of cholesterol monohydrate spherulites. (a-c) Microscopic morphology of cholesterol monohydrate spherulites extending outward from the crystal nucleus. (d) Monohydrate cholesterol microcrystals in spherulites.

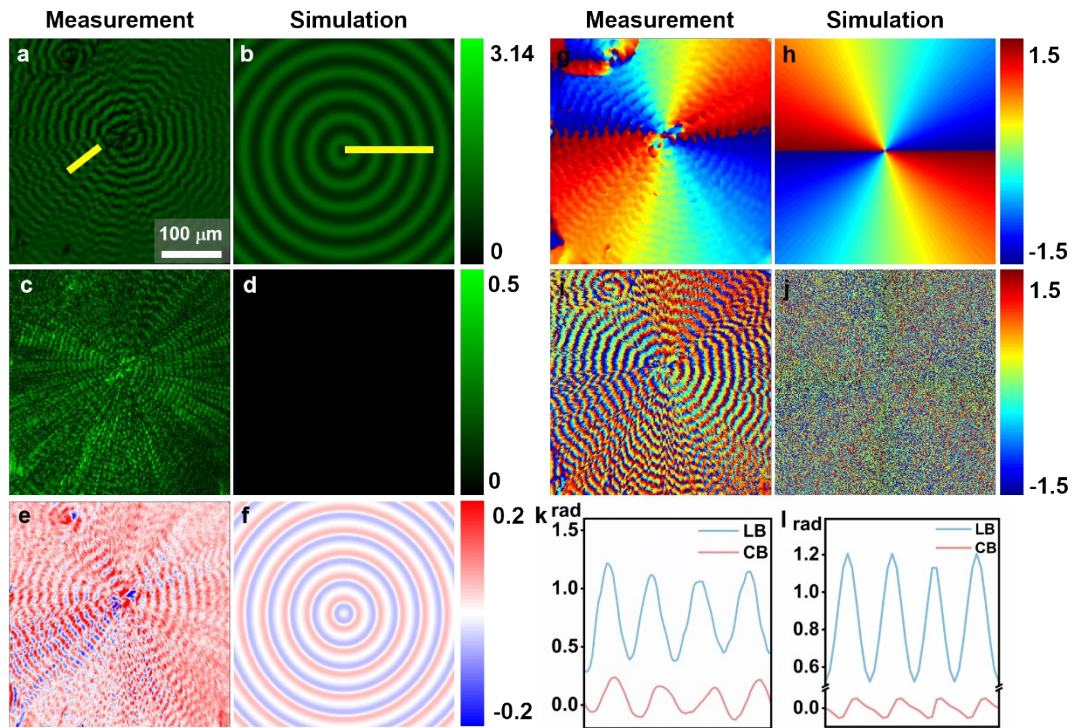


Fig. S5 Experimental and simulated optical results of banded cholesterol polymorph I ( $\lambda = 530$  nm): measured  $|LB|$  (a),  $|LD|$  (c), CB(e), LB angle (g) and LD angle (i) images and their corresponding simulation results on the right. (k-l) The extracted optical properties along the yellow lines for polymorph I and simulation diagram. For (i-j), scattering from the assembled cholesterol crystalline fibers.

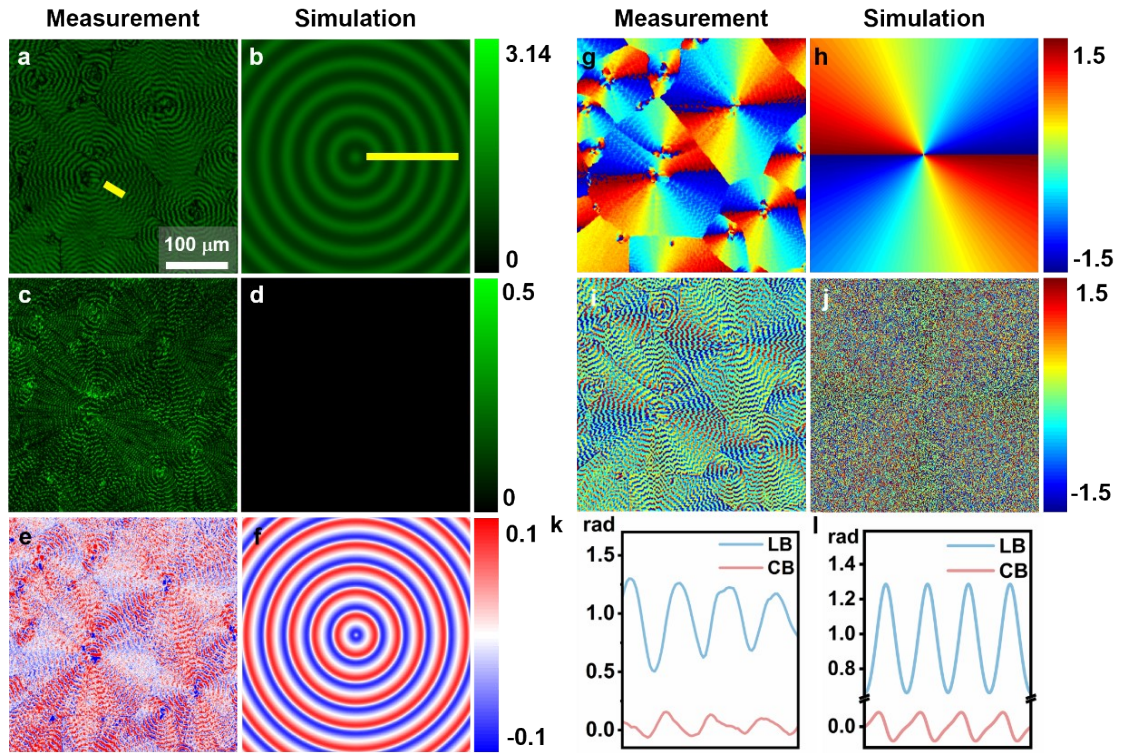


Fig. S6 Experimental and simulated optical results of banded cholesteral polymorph II ( $\lambda = 530 \text{ nm}$ ): measured  $|LB|$  (a),  $|LD|$  (c), CB(e), LB angle (g) and LD angle (i) images and their corresponding simulation results on the right. (k-l) The extracted optical properties along the yellow lines for polymorph I and simulation diagram. For (i-j), scattering from the assembled cholesteral crystalline fibers.

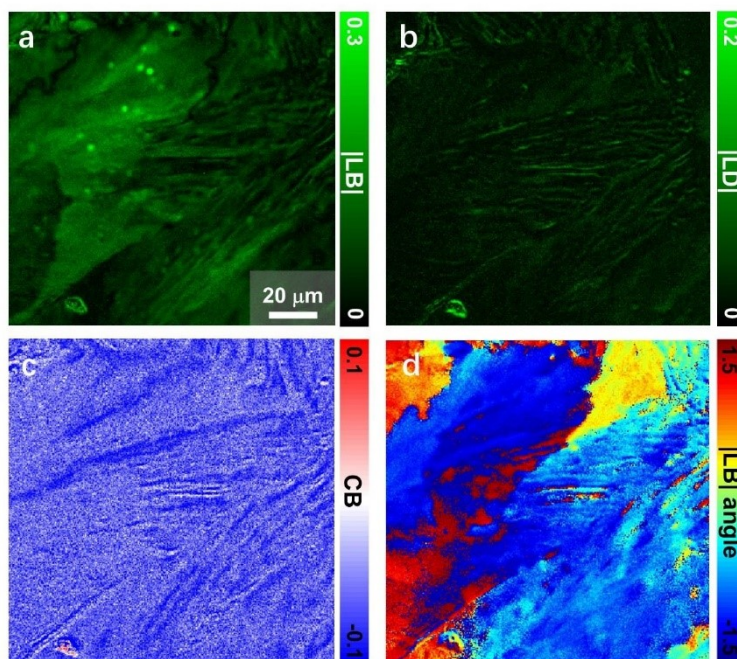


Fig. S7 Experimental optical results of monohydrate cholesterol spherulites ( $\lambda = 530$  nm). (a) LB, (b) LD, (c) CB, (d) LB angle images.

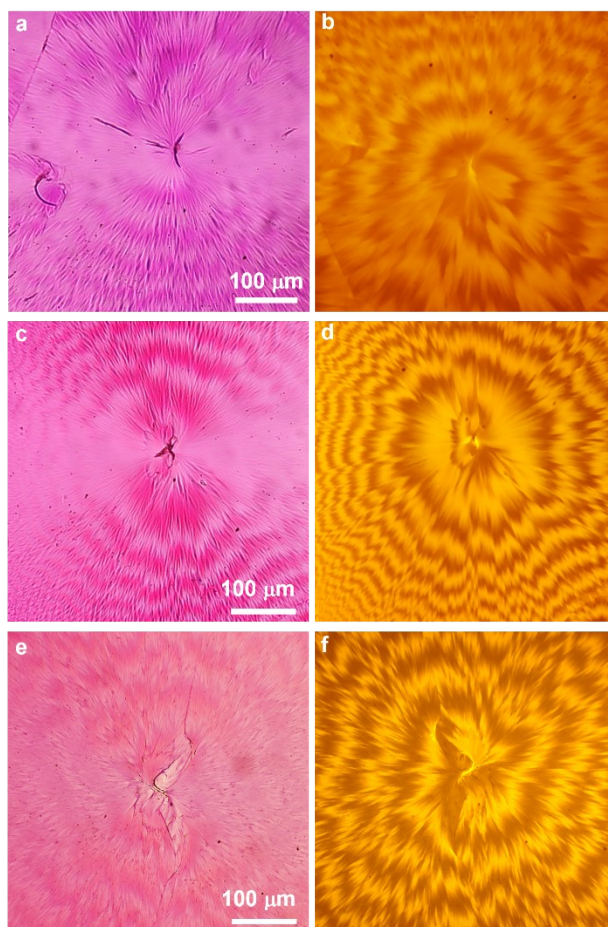


Fig. S8 Stained cholesterol banded spherulites and their corresponding fluorescent images. (a, c, e) coumarin, Rhodamine 6G, Oil Red O stained cholesterol banded spherulites images with dyes arranged perpendicular to the radii under horizontally polarized light. (b, d, f) Fluorescent images of the corresponding polarized micrographs on the left.

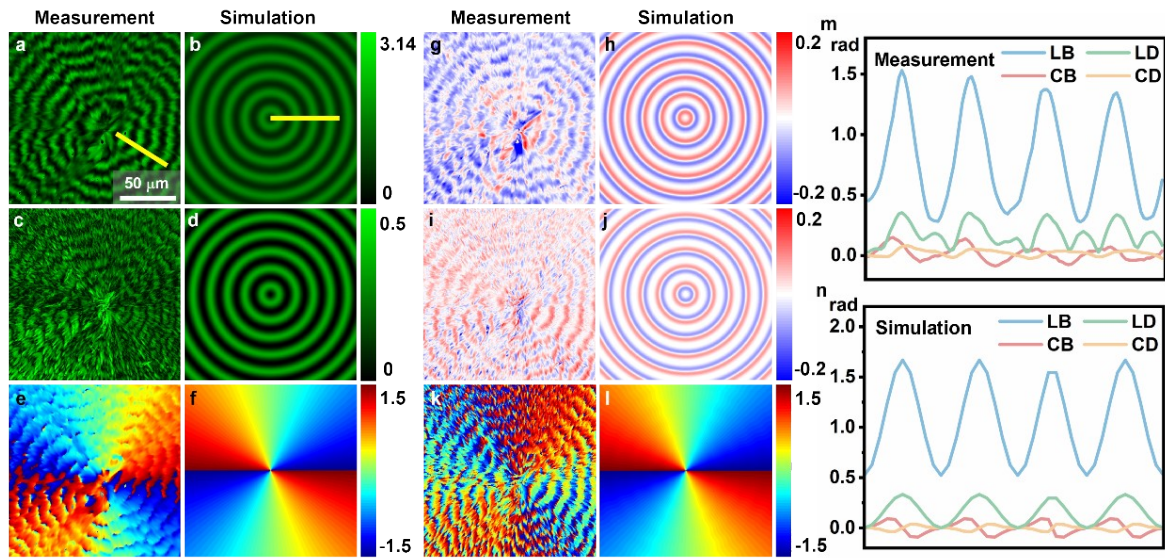


Fig. S9. Experimental and simulated optical results of stained banded cholesteral polymorph I. (a-l) Measured (a)  $|LB|$ , (c)  $|LD|$ , (g) CB, (i) CD, (e) LB angle and (k) LD angle images of stained polymorph I ( $\lambda = 550$  nm) and its corresponding simulation results on the right. (m-n) The extracted optical properties along the yellow lines for stained polymorph I and simulation diagram.

## 5. Reference

1. X. Feng, T. Wang, M. Hao, N. Xue, H. Zhu, Y. Tian and X. Cui, *ChemComm*, 2023, **59**, 3297-3300.
2. X. Cui, S. M. Nichols, O. Arteaga, J. Freudenthal, F. Paula, A. G. Shtukenberg and B. Kahr, *J. Am. Chem. Soc.*, 2016, **138**, 12211-12218.
3. L. N. Poloni, Z. Zhu, N. Garcia-Vázquez, A. C. Yu, D. M. Connors, L. Hu, A. Sahota, M. D. Ward and A. G. Shtukenberg, *Cryst. Growth. Des.*, 2017, **17**, 2767-2781.